

# High-Level Sprout Geometry Extraction for In Vitro Angiogenesis Assays

Gio Borje  
University of California, Irvine  
gborje@uci.edu

Craig Steinke  
University of California, Irvine  
steinkec@uci.edu

## ABSTRACT

We have developed an automated system for the quantitative analysis of *in vitro* angiogenesis assays. Specifically, the system is designed to analyze fibrin gel bead sprouting assays developed by the laboratory of Dr. Chris Hughes in the Department of Molecular Biology & Biochemistry at UC Irvine. Our system enumerates sprouts for each bead and calculates the average length for an imaged assay. Our approach reports accurate sprout enumeration when compared with manual counts by an expert observer while significantly reducing the analysis time.

## 1. INTRODUCTION

Angiogenesis is a mechanism for the formation of new blood vessels from pre-existing vessels. Tumor angiogenesis in solid tumors is thought to facilitate the transition from a benign tumor to a malignant phenotype. Additionally, the avascular growth phase allows for an approximate maximum size of 1–2mm in diameter; on the other hand, the vascular growth phase enables unyielding tumor expansion and metastasis [3]. Subsequently, the analysis of *in vitro* angiogenesis assays is necessary to assess the impact of pro-angiogenic and anti-angiogenic agents.

Niemisto et. al developed a general image analysis method for the quantification of similar *in vitro* angiogenesis assays. Their method provides the length and size of each tubule complex as well as the number of junctions within them [5]. The TCS Cellworks Angiokit (Buckingham, UK) images used by Niemisto et. al have two distinguishable and ideal properties in contrast to our images that require us to use a variant approach. First, their images have tubule complexes that are solidly filled whereas our images have visible lumens. Second, their images show no distinguishable origin for sprouts whereas our images have a bead from which sprouts originate. Hence, we propose a modified methodology for our image set.

The image set under analysis is provided by the Hughes Lab. Their fibrin bead assay using human umbilical vein endothelial cells (HUVEC) contrasts with fibrin bead assays containing Bovine aortic endothelial cells (BAEC). HUVEC have been the canonical EC model system and more accurately represents angiogenesis in humans. The assay

begins by culturing HUVEC as a monolayer on dextran-coated Cytodex beads. This method induces HUVEC to recapitulate multicellular capillaries in fibrin gels. Furthermore, the method for HUVEC promotes sprouting, lumen formation and long-term stability of neovessels. The high-resolution images of beads are then captured on an IX70 Olympus microscope [4]. A sample image can be seen on Figure 1.

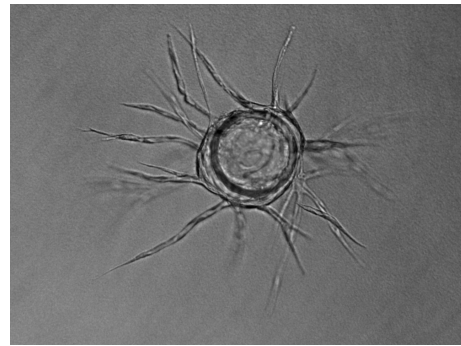


**Figure 1: Single Bead Image from the Hughes Lab Images**

Components of an image are described as follows. A *bead* refers to the Cytodex bead. The *sprouts* are the multicellular capillary structures formed by endothelial cells. The *sprout count* refers to the number of sprouts per bead. For quantitative analysis, the objective of the system is to yield sprout counts that are consistent with an expert observer.

Previously, the number of sprout counts per bead were measured by manual counting on the obtained images. Furthermore, the sprout length was ambiguously measured in arbitrary units [4]. Our system relieves the laborious, manual analysis by quickly automating the detection and reliably analyzing of imaged assay features.

Our system, the High-Level Sprout Geometry (HLSG) Extractor, is designed to detect high-level object and analyze the objects of imaged assays. Objects for detection include the Cytodex bead and its associated multicellular capillaries. Due to the noise and depth of the image, the HLSG Extractor uses structural inpainting to infer which sprout segments emerge belong the same sprout. After structural

inpainting, the HLSG Extractor quantitatively analyzed the images using Sholl Analysis to determine the number of primary sprouts and the average length for each bead in the imaged assay.

In addition to the High-Level Sprout Geometry (HLSG) Extractor, a driver and report generator are implemented to drive functionality on sample images and generate reports on the analyses respectively.

The following sections will proceed as follows. Section 3 will describe an overview of the HLSG feature detection and analysis mechanisms. Section ?? will describe the data structures used to represent the HLSG and its properties. Section 2 shows how the system is designed for modularity and robustness.

## 2. SYSTEM ARCHITECTURE

The system requires Python version 2.7x with the SimpleCV package. The architecture of the system is based on our methodology for quantitatively analyzing *in vitro* angiogenesis. The system, however, incorporates modules for driving batch processes as well as a Read-Eval-Print-Loop (REPL) for console interaction. Finally, a module incorporated for generating CSV reports of the analysis. The sequence diagram for the system components are shown in Figure 2.

## 3. METHODOLOGY

Our system enables detection of high-level features and quantitative analysis of morphometrics which can be decomposed into four stages. The first stage is preprocessing: obtain a black and white image such that the foreground only contains two objects of interest: beads and sprout segments. The second stage is bead detection where the system finds the origin and radius of each bead in the image. The third stage is non-bead detection where the system collects all sprout segments from the image. Once the sprout segments are collected, the system adjusts the sprout segments to reduce noise in the analysis stage. The system begins by restoring holes and small gaps within sprout segments. Second, spurious arcs and noise are pruned. Finally, the resulting image is analyzed through Sholl Analysis which collects the number of crossings for a set of concentric circles with a fixed origin as the origin of a detected bead.

### 3.1 Preprocessing

In the preprocessing step, the system converts the image into a black and white image where white represents the foreground and black represents the background. Objects in the foreground are elements of interest. Specifically, a foreground object can belong one of three higher-order objects: a bead, a sprout segment or noise. Noise is an artifact generated from the original image as well as the image processing techniques. We use the Canny edge detection algorithm [2] to obtain the black and white images

such the edges represent the contours of the elements of interest.

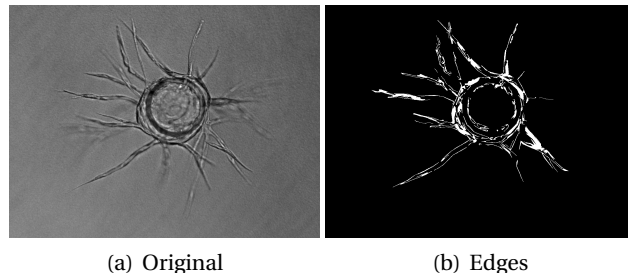


Figure 3: Edge Detection Outline

### 3.2 Bead Detection

Bead detection is a three-step process. To reduce noise, the system first smooths the image using a Gaussian blur. Next, the system obtains a black and white version of the image through the edges of the image using the Canny edge detection algorithm. Finally, circles in the image are detected using the circular Hough Transform [7]. The circles detected correspond to the beads in the imaged assay. It follows that the origin and radius of the bead are obtained.

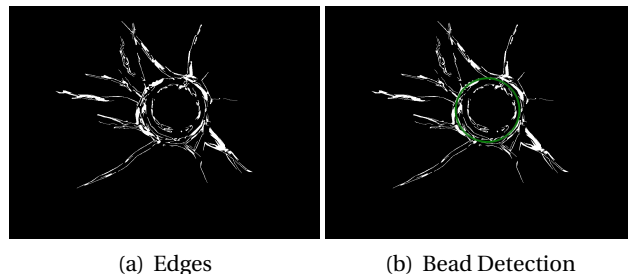


Figure 4: Bead Detection Outline

In order to avoid false bead detections, we enforce that the minimum distance between the origin of every pair of detected circles be four times the average bead radius while preferring beads with the more votes in the accumulator i.e. each detected bead should at least be a bead apart. We ignore the degenerate case in which two or more beads are within the distance constraint because associating sprouts to beads becomes inaccurate.

### 3.3 Non-Bead (Sprout) Detection

The system begins by obtaining a black and white image from the grayscale imaged assay. Since the edges of the images represent the contours of beads, sprouts and noise, we mask the detected beads such that only the sprout and noise contours remain. The noise is reduced in the sprout restoration phase.

Since the borders of the sprouts are detected as edges, they may appear to be distinctly segmented objects. We

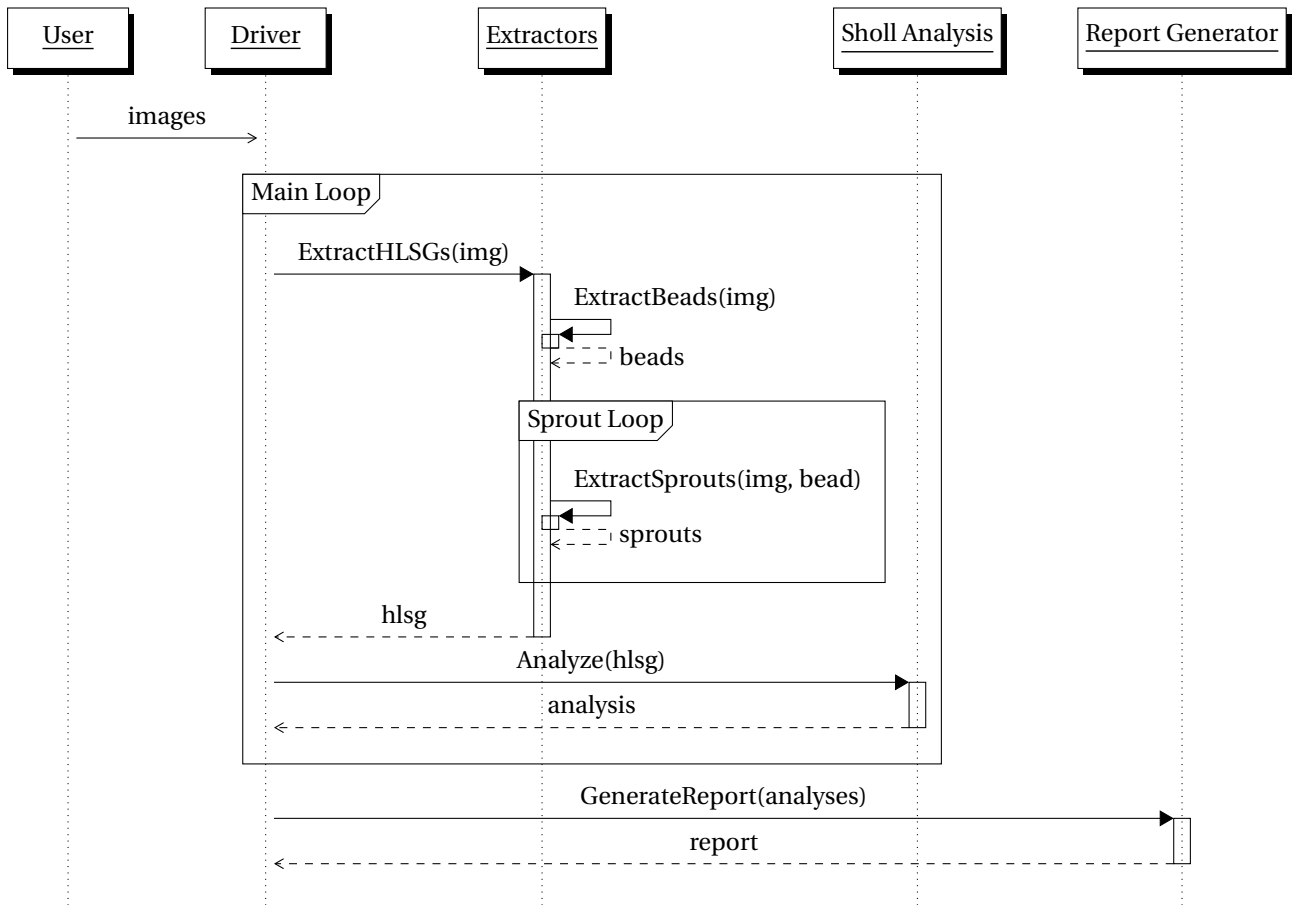
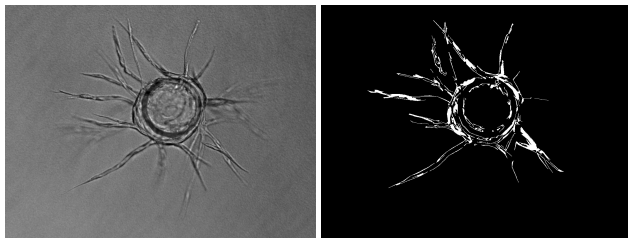


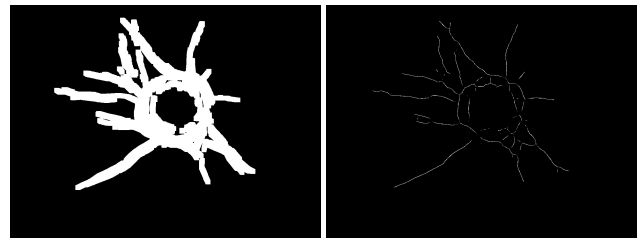
Figure 2: High-Level Architecture



(a) Original

(b) Edges

Figure 5: Edge Detection Outline



(a) Thickening

(b) Thinning and Pruning

Figure 6: Sprout Detection Outline without Bead Masks

call such objects *sprout segments*. Subsequently, it is necessary that the system links the sprout segments to reconstruct the original sprout.

The system approaches the reconstruction by first thickening the sprout segments until the lumen disappears. Next, the thickened structure is skeletonized by thinning. Since the skeleton represents the fundamental morphology of the structure, and approximate centerline for each of the sprouts are generated. We now utilize the disjoint centerlines as sprout segments.

### 3.3.1 Sprout Segment Connectivity

Due to the discontinuity of sprouts in the assay, we begin by collecting all sprout segments and represent them as line segments. We distinguish the end points of each line segment as either an inner point or outer point. The inner point,  $I$ , is the end point on the line segment such that it is closer to the origin of the line segment's closest bead. The outer point,  $O$ , is the end point on the line segment such that it is farther from the origin of the line segment's closest bead.

To determine which line segments belong to the same sprout, we use Euclidean distance between their inner and outer points enforced by the constraint that the end point must be closer to the origin of its closest bead than the target start point. For example, two line segments are part of the same sprout if the distance between the start and end points are within a specified distance parameter,  $d$ .

Once the sprouts segments have been connected, we refer to the connected structures as sprouts.

### 3.3.2 Sprout Restoration

In this phase, there are two primary sources of degradation observed. First, noise is still in the foreground after sprouts segments are connected. Second, holes may exist in the morphology of the sprouts after thickening and thinning the structures. We describe our methods for resolving each problem independently.

Noise in the image can be described in two common forms: isolated points and spurious arcs. Isolated points refer to the small objects detected in the foreground that have no apparent relation to sprout segments. Spurious arcs are auxiliary stubs that are generated from skeletonization. To remove the noise from the black and white image, we apply several hit-and-miss transformation that masks isolated points and spurious arcs. Hence, only the sprout segments remain.

$$\begin{pmatrix} -1 & -1 & -1 & -1 & -1 \\ -1 & 0 & 0 & 0 & -1 \\ -1 & 0 & 1 & 0 & -1 \\ -1 & 0 & 0 & 0 & -1 \\ -1 & -1 & -1 & -1 & -1 \end{pmatrix}$$

**Figure 7: Hit-and-Miss Transformation Kernel for Isolated Points where 1 represents foreground, -1 represents background and 0 can be either**

In contrast with noise, holes are points that can be found within foreground structures that should have been detected as foreground. These holes are primarily artifacts of the Canny edge-detection algorithm since the contours of a capillary encompass the lumen which is detected as background. By the morphology of these structures, we simply find the contours which enclose small holes and perform inpainting.

## 3.4 Sholl Analysis

Sholl Analysis is a quantitative method for quantitatively analyzing morphological characteristics of neurons [6]. We use Sholl Analysis because the morphology of our imaged assays closely resembles neuron images after our preprocessing steps.

Briefly, Sholl Analysis consists of counting the number of foreground to background crossings given concentric circles of a centered at the origin of a bead. The algorithm

can then be decomposed into initialization, iteration and final stages. For the initialization, we select a bead,  $B$ . Next, let the initial circle radius,  $r_{\min}$ , be slightly larger than the detected radius of the bead and let the maximum radius,  $r_{\max}$ , be the minimum distance from the origin of the detected bead to either of the four image borders. For each radius,  $r \in [r_{\min}, r_{\max}]$ , we define the number of crossings as  $N(r)$ . For further analysis, we define the critical value,  $CV(N)$ , as the radius at which the maximum number of crossings occur. See A.1 for the pseudo code using an optimized Bresenham Circle Algorithm.

For posterior analysis, we define longest increasing subsequence (LIS) of  $N(r)$  as  $LIS(N)$  with the domain constrained between  $[r_{\min}, CV(N)]$ . The longest decreasing subsequence (LDS),  $LDS(N)$  is defined similarly with the domain constrained to  $[CV(N), r_{\max}]$ . The LIS and LDS guarantee that we have strictly increasing counts to ignore gaps as noise.

From the number of crossings, we determine the sprout counts and average length. The sprout counts,  $c_N$ , are determined by a median of the  $LIS(r)$ . To determine the average length,  $l_N$ , we define a procedure. First, we define by the radius at which  $LDS(N)$  has a value of 1 as  $l_{\max}$  and we define the radius at which  $LDS(N)$  has a value of  $c_N$  as  $l_{\min}$ . Then, we calculate  $l_N$  as the average of  $l_{\max}$  and  $l_{\min}$ .

## 4. RESULTS

The results of our sprout counts show a standard error of 1.7 when compared manual sprout counts of an expert observer (see Table 1). In the table, the expert observer sprout counts include only sprouts which are declared to be in-focus.

Treatment	Human Counts	HLSG Counts
10k 1 Day 7	7	10
10k 5 Day 7	10	10
1k 2 Day 7	11	9
1k 3 Day 7	14	14
20k 1 Day 7	15	10
20k 2 Day 7	15	12
20k 3 Day 7	6	8
20k 5 Day 7	9	10
Ang1 100 ng/ml 3 Day 7	7	9
Ang1 100 ng/ml 5 Day 7	9	12
Ang1 250 ng/ml 1 Day 7	8	7
Control 1 Day 7	10	12
Control 2 Day 7	12	13
Control 4 Day 7	8	8
Control 5 Day 7	7	9

**Table 1: Expert Observer vs. HLSG Sprout Counts**

The average lengths have also been obtained with arbitrary units; however, there currently exists no average length data from an expert observer for comparison.

## 5. DISCUSSION

The sprout count results demonstrate consistency with human observers for in focus sprouts. Our HLSG Extractor, however, also shows a consistent pattern in overestimating the number of sprouts declared to be in-focus by an expert observer. This occurs because our system may also capture sprouts that were declared to be out-of-focus by an expert observer. The preprocessing phase of our methodology uses edge detection to determine which sprouts to count whereas an expert observer may utilize other features beyond a discernable cell wall.

Furthermore, we speculate that sprouts crossings and sprout discontinuities are the greatest sources of error in sprout counts. Sprout crossings are defined to be the occurrence of two overlapping sprouts. A method of effectively distinguishing sprout branching from sprout crossings is still an open problem. Additionally, more effective sprout restoration methods could improve the accuracy of Sholl Analysis.

## 6. CONCLUSIONS

Automated image analysis methods are necessary for the assessment of pro-angiogenic and anti-angiogenic agents in an *in vitro* angiogenesis assay. Unfortunately, the methodology of contemporary software is insufficient for our data set. Manual methods are also laborious and vulnerable to observer bias.

To overcome these shortcomings, we have designed an optimized image analysis method for quantitatively analyzing *in vitro* angiogenesis assays containing HUVEC. The system, HLSG Extractor, obtains sprout counts that are consistent with the accuracy of an expert observer. In addition to sprout counts, the average length of the sprouts per bead have are also obtained. With the versatility of Sholl Analysis, several other morphometrics may become available using further statistical methods.

Potential adjustments to the system may include new implementations and different approaches to the phases of the optimized methodology. For example, given the sprout counts of the bead of an imaged assay, we may reduce the noise from discontinuous sprouts further by a piecewise constant approximation of the sprout counts. Subsequently, methods of integration may be unnecessary.

Cumulatively, the HLSG Extractor has proven to be a consistent, robust and automated image analysis system of *in vitro* angiogenesis morphology.

## 7. ACKNOWLEDGEMENTS

We would like to thank Dr. Ernie Esser and Anna Konstorum from the Department of Mathematics, University of California, Irvine, for valuable commentary and guidance throughout the research process. We would also like to acknowledge the laboratory of Dr. Chris Hughes in the Department of Molecular Biology & Biochemistry at UC Irvine for making available the image sets of their fibrin

gel bead sprouting assays. This research was funded by the National Science Foundation (NSF) DMS-0928427.

## 8. REFERENCES

- [1] Jack Bresenham. A linear algorithm for incremental digital display of circular arcs. *Commun. ACM*, 20(2):100–106, February 1977.
- [2] J Canny. A computational approach to edge detection. *IEEE Trans. Pattern Anal. Mach. Intell.*, 8(6):679–698, June 1986.
- [3] Robert S. Kerbel. Tumor angiogenesis: past, present and the near future. *Carcinogenesis*, 21(3):505–515, 1999.
- [4] Martin N. Nakatsu, Richard C.A. Sainson, Jason N. Aoto, Kevin L. Taylor, Mark Aitkenhead, Sofía Pérez del Pulgar, Philip M. Carpenter, and Christopher C.W. Hughes. Angiogenic sprouting and capillary lumen formation modeled by human umbilical vein endothelial cells (huvec) in fibrin gels: the role of fibroblasts and angiopoietin-1. *Microvascular Research*, 66(2):102 – 112, 2003.
- [5] A. Niemisto, V. Dunmire, O. Yli-Harja, Wei Zhang, and I. Shmulevich. Robust quantification of in vitro angiogenesis through image analysis. *Medical Imaging, IEEE Transactions on*, 24(4):549–553, 2005.
- [6] D. A. Sholl. Dendritic organization in the neurons of the visual and motor cortices of the cat. *J Anat.*, 87(4):387–406, 1953.
- [7] H. K. Yuen, J. Princen, J. Dlingworth, and J. Kittler. A comparative study of hough transform methods for circle finding. In *Proc. AVC*, pages 29.1–29.6, 1989. doi:10.5244/C.3.29.

## APPENDIX

### A. PSEUDO CODE

This section outlines the pseudo code for Sholl Analysis by using an optimized Bresenham Circle Algorithm for circular point generation.

#### A.1 Sholl Analysis

Sholl Analysis counts the number of crossings for a set of concentric circles from an initially defined radius to a maximally defined radius. See Algorithm 1 for our precise implementation.

#### A.2 Ordered Bresenham Circle Algorithm

Bresenham’s circle algorithm is frequently used to determine which pixels should be selected to draw a circle. algorithm utilizes symmetry of a circle in order to reduce the running time by a factor of eight [1]. For our application with Sholl Analysis, the algorithm must return the points as an ordered set which is defined to be counterclockwise starting from the positive x-axis.

The algorithm calculates points for all eight octants simultaneously. The octants are labeled with integers start-

---

**Algorithm 1** Sholl Analysis

---

```
procedure SHOLLANALYSIS(img, origin, radius)
   $r_{\min} \leftarrow \text{radius}$ 
   $r_{\max} \leftarrow \min\{\text{origin.x}, \text{img.width} - \text{origin.x}\}$ 
   $r_{\max} \leftarrow \min\{r_{\max}, \text{origin.y}, \text{img.height} - \text{origin.y}\}$ 
  crossings  $\leftarrow$  empty dictionary
  for all  $r \in [r_{\min}, r_{\max}]$  do
    crossings[ $r$ ]  $\leftarrow$  COUNTCROSSINGS(img, origin,  $r$ )
  end for
  return crossings
end procedure

procedure COUNTCROSSINGS(img, origin, radius)
  crossings  $\leftarrow$  0
  for all pixel  $\in$  BRESENHAMCIRCLE(origin, radius) do
    if crossing detected at pixel then
      crossings  $\leftarrow$  crossings + 1
    end if
  end for
  return crossings
end procedure
```

---

ing with zero. We label the octants from starting from the x-positive axis in the counterclockwise direction. The labels can be seen in figure 8. Because it is necessary that

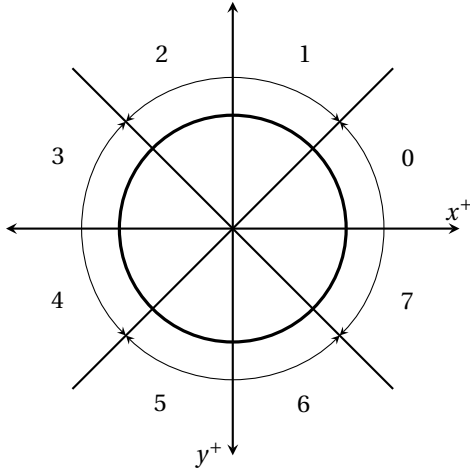


**Figure 8: Octants in the Eight-Way Symmetry of a Circle**

the points are ordered counterclockwise from the positive x-axis, we modify the algorithm. The algorithm calculates the points from ordered clockwise or counterclockwise from the closest coordinate axis. Hence, we reverse the points calculated for every odd octant and then concatenate their data points.

---

**Algorithm 2** Ordered Bresenham Circle Algorithm

---

**Ensure:** points returned are ordered counterclockwise from the positive x-axis

```
procedure BRESENHAMCIRCLE(origin, radius)
```

```
   $x \leftarrow \text{radius}$ 
   $y \leftarrow 0$ 
   $r_{\text{error}} \leftarrow 1 - x$ 
  octants  $\leftarrow$  empty array
  while  $x \geq y$  do
    octants[0]  $\leftarrow (x + \text{origin.x}, -y + \text{origin.y})$ 
    octants[1]  $\leftarrow (y + \text{origin.x}, -x + \text{origin.y})$ 
    octants[2]  $\leftarrow (-y + \text{origin.x}, -x + \text{origin.y})$ 
    octants[3]  $\leftarrow (-x + \text{origin.x}, -y + \text{origin.y})$ 
    octants[4]  $\leftarrow (-x + \text{origin.x}, y + \text{origin.y})$ 
    octants[5]  $\leftarrow (-y + \text{origin.x}, x + \text{origin.y})$ 
    octants[6]  $\leftarrow (y + \text{origin.x}, x + \text{origin.y})$ 
    octants[7]  $\leftarrow (x + \text{origin.x}, y + \text{origin.y})$ 
     $y \leftarrow y + 1$ 
    if  $r_{\text{error}} < 0$  then
       $r_{\text{error}} \leftarrow r_{\text{error}} + 2y + 1$ 
    else
       $x \leftarrow x - 1$ 
       $r_{\text{error}} \leftarrow r_{\text{error}} + 2(y - x + 1)$ 
    end if
  end while
  points  $\leftarrow []$ 
  for all octant  $\in$  octants do
    if octant is odd then
      reverse the octant
    end if
    for all point  $\in$  octant do
      points  $\leftarrow$  point
    end for
  end for
  return points
end procedure
```

---